Supporting Information

Mixed organic cations promote ambient light-induced formation of metallic lead in lead halide perovskite crystals

Aniruddha Ray,[1,2] Beatriz Martín-García,[1,3,4] Mirko Prato,[1] Anna Moliterni,[5] Simone Bordignon,[6] Davide Spirito,[7] Sergio Marras,[1] Luca Goldoni,[1] Karunakara Moorthy Boopathi,[1] Fabrizio Moro,[8] Nicola Pietro Maria Casati,[9] Carlotta Giacobbe,[10] Makhsud I. Saidaminov,[11] Cinzia Giannini,[5] Michele R. Chierotti,[6] Roman Krahne,[1] Liberato Manna,[1,*] Ahmed L. Abdelhady[1,12, 13*]

[1]Istituto Italiano di Tecnologia, Via Morego 30, 16163 Genova, Italy

[2]RGS Development B.V. Bijlestaal 54a, Broek op Langedijk 1721 PW, Dijk en Waard, Netherlands

[3]CIC nanoGUNE, Tolosa Hiribidea, 76, 20018 Donostia-San Sebastian, Spain

[4]IKERBASQUE, Basque Foundation for Science, 48009 Bilbao, Spain

[5]Istituto di Cristallografia, Consiglio Nazionale delle Ricerche, Via Amendola 122/O, 70126 Bari, Italy

[6]Department of Chemistry, University of Torino, 10125 Torino, Italy

[7]IHP—Leibniz-Institut für innovative Mikroelektronik, Im Technologiepark 25, D-15236 Frankfurt (Oder), Germany

[8]Dipartimento di Scienza dei Materiali, Università degli Studi Milano-Bicocca, Milano 20125, Italy

[9]Laboratory for Synchrotron Radiation—Condensed Matter, Paul Scherrer Institut, 5232 Villigen, Switzerland

[10]European Synchrotron Radiation Facility, 71 Avenue Des Martyrs, Grenoble 38040, France

[11]Department of Chemistry, University of Victoria, Victoria, British Columbia V8P 5C2, Canada

[12]Department of Chemistry Khalifa University P.O. Box 127788, Abu Dhabi, United Arab Emirates

[13]Advanced Materials Chemistry Center (AMCC) Khalifa University P.O. Box 127788, Abu Dhabi, United Arab Emirates

*Corresponding author: liberato.manna@iit.it and ahmed.abdelhady@ku.ac.ae

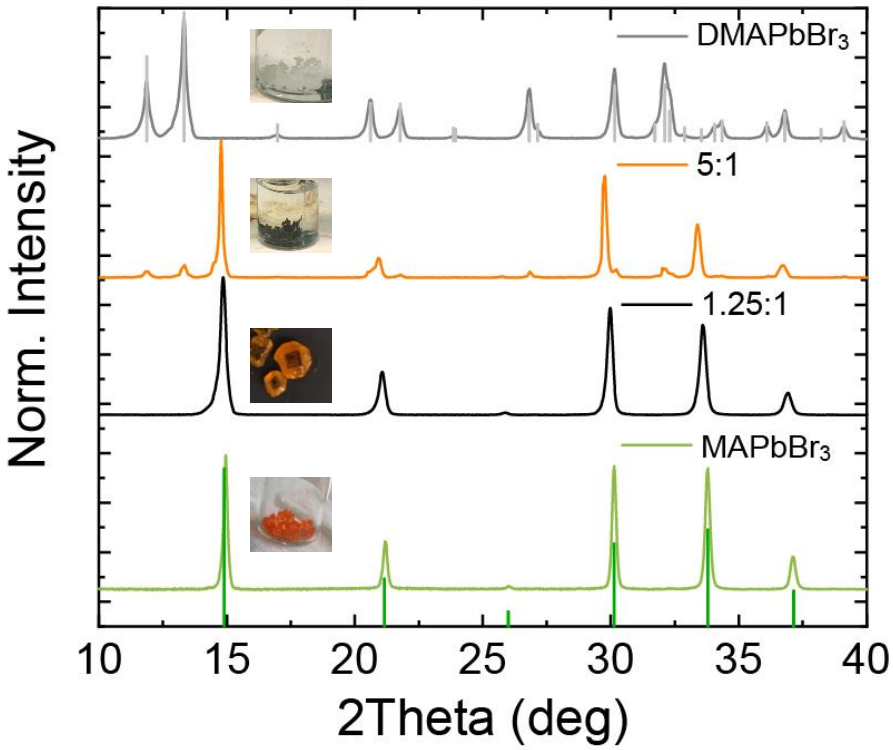

Figure S1. LXRPD on ground powders of $DMAPbBr_3$, $MAPbBr_3$ and mixed (1.25:1 and 5:1) DMA/$MAPbBr_3$ crystals that are grown using the SAC process compared to the cubic $MAPbBr_3$ (ICSD 268785; green lines) and the non-perovskite $DMAPbBr_3$ phase (ICSD 402591; gray lines).

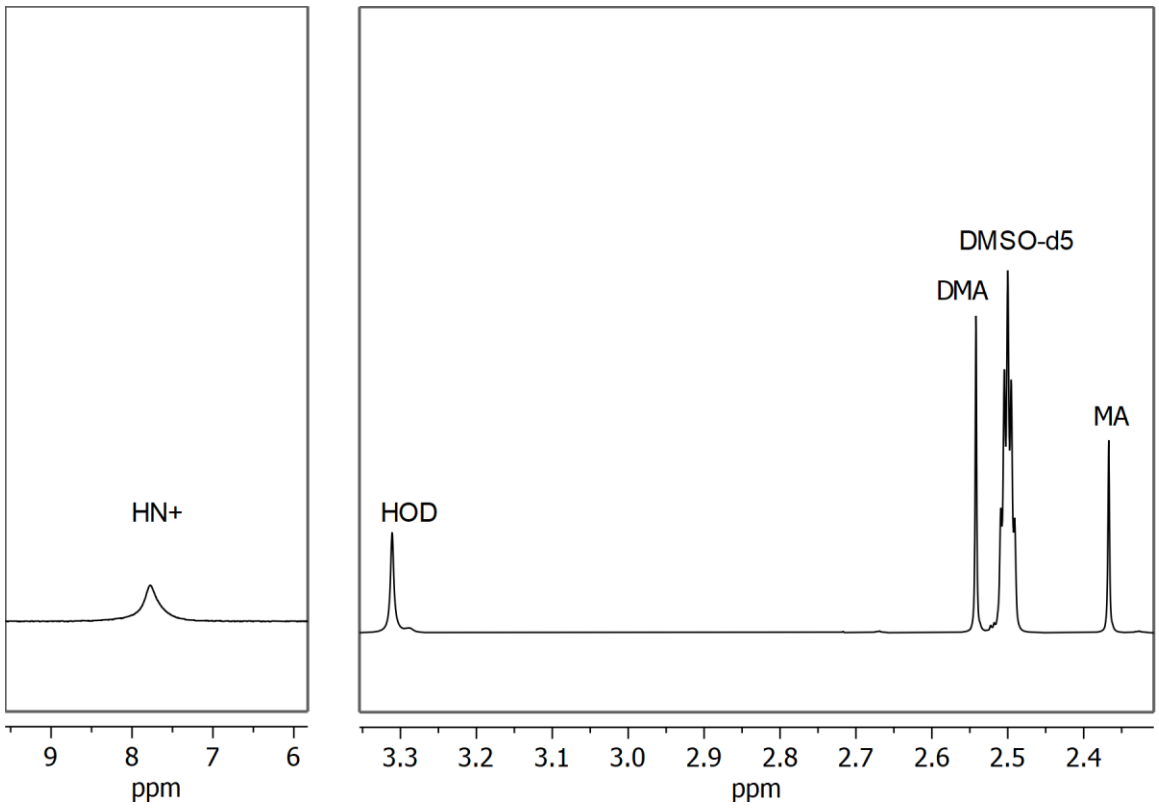

Figure S2. Liquid-state ^{1}H NMR of the black crystals, collected after 4 days, by dissolving the crystals in deuterated DMSO.

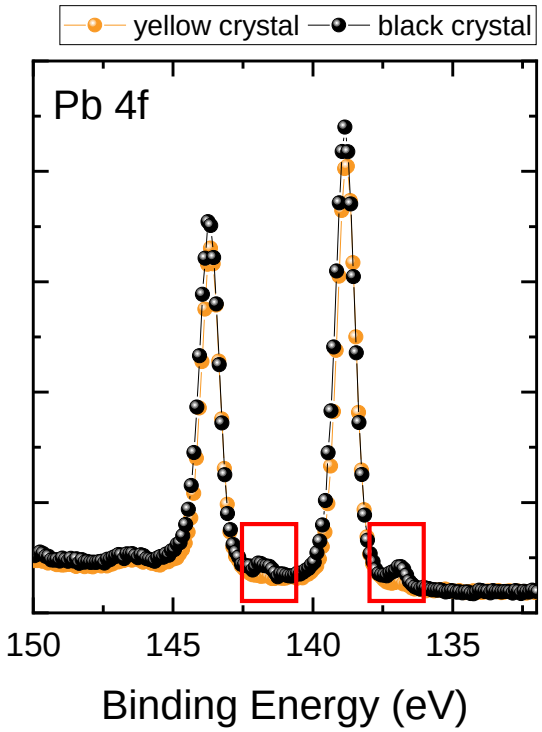

Figure S3. XPS spectra of Pb 4f of both yellow and black crystals – red boxes highlight Pb(0) peak.

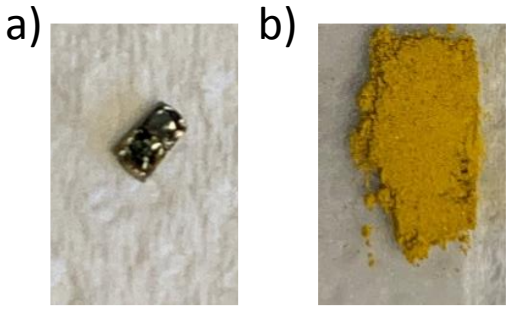

Figure S4. Photographs of (a) cleaved surface and (b) ground powder of a black DMA/$MAPbBr_3$ crystal.

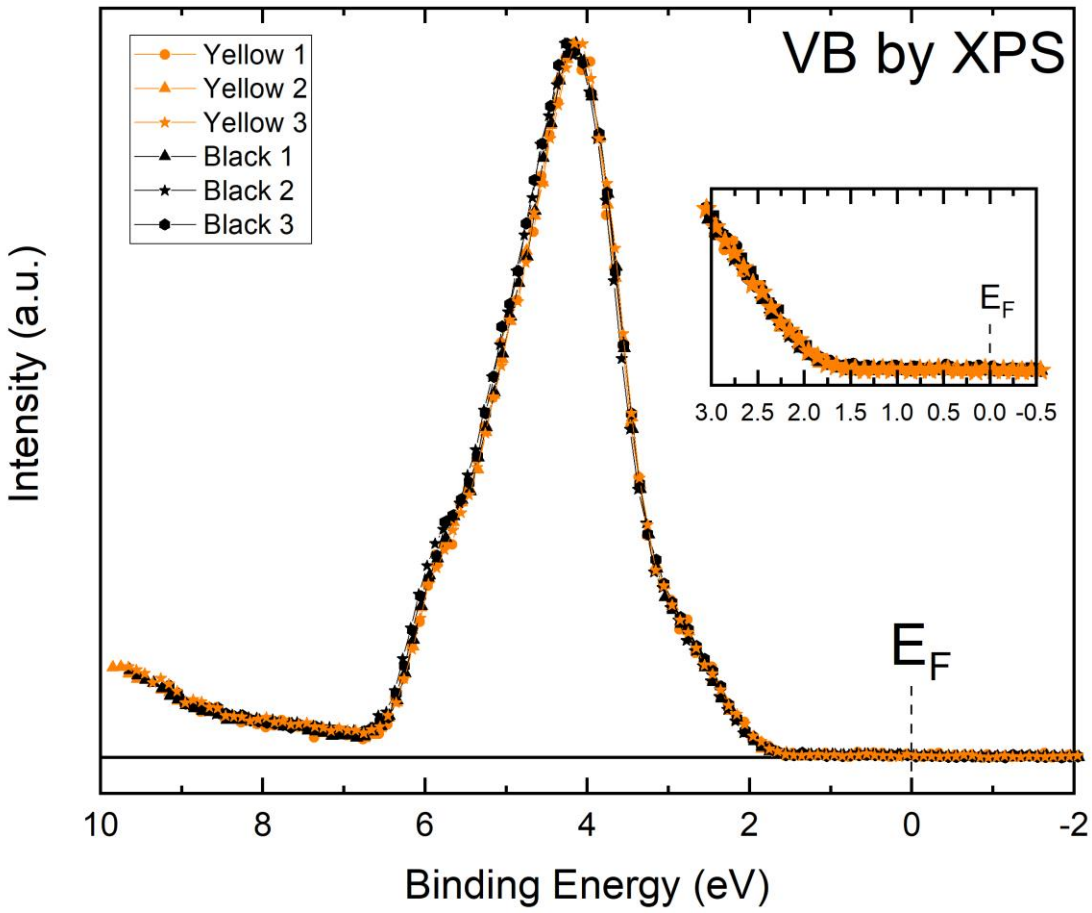

Figure S5. XPS showing the valence band region of both yellow and black crystals. Data collected on three different samples are shown for both crystals.

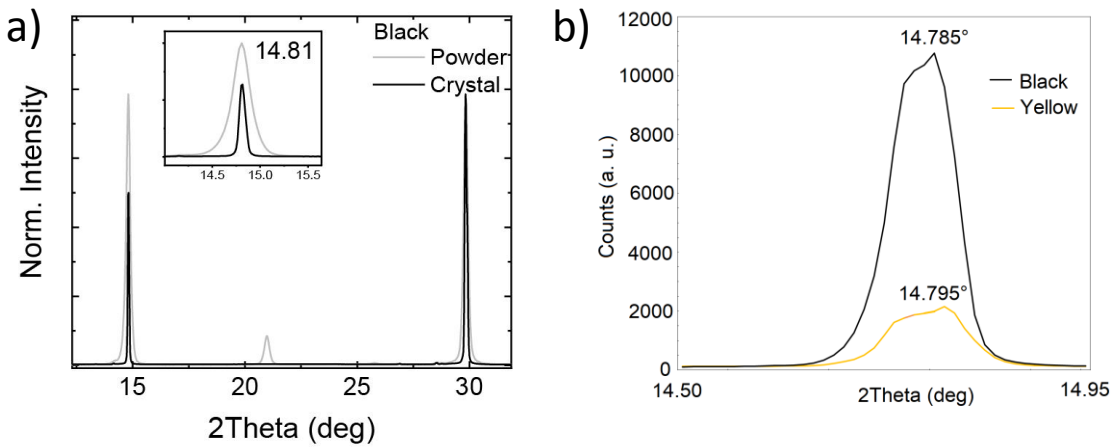

Figure S6. (a) LXRPD patterns of as-grown black crystals and their powders and (b) zoomed-in view of the SXRPD patterns collected on powders derived from grinding black and yellow crystals. The SXRPD profiles are plotted in the Cu-Kα 2θ scale to ease the comparison with lab-grade diffraction patterns.

Table S1. Crystal systems, space groups and cell axes at selected temperatures of ground yellow and black crystals.

	Yellow $((CH_3)_2NH_2)(CH_3NH_3)PbBr_3$ (Mixed DMA/$MAPbBr_3$)		**Black $((CH_3)_2NH_2)(CH_3NH_3)PbBr_3$ (Mixed DMA/$MAPbBr_3$)**	
Temperature (K)	**Crystal system Space group**	**Cell axes (Å)**	**Crystal system Space group**	**Cell axes (Å)**
300	Cubic *Pm*-3*m*	*a* = *b* = *c* = 5.98323(18)	Cubic *Pm*-3*m*	*a* = *b* =*c* = 5.98416(5)
240	Cubic *Pm*-3*m*	*a* = *b* = *c* = 5.966158(11)	Cubic *Pm*-3*m*	*a* = *b* = *c* = 5.97113(5)
220	Cubic *Pm*-3*m*	*a* = *b* = *c* = 5.96089(12)	Cubic *Pm*-3*m*	*a* = *b* = *c* = 5.96573(5)
205	Cubic *Pm*-3*m*	*a* = *b* = *c* = 5.95844(9)	Cubic *Pm*-3*m*	*a* = *b* = *c* = 5.96112(5)
200	Tetragonal *P*4/*mbm*	*a* = *b* = 8.4191(9) *c* = 5.9535(19)	Tetragonal *P*4/*mbm*	*a* = *b* = 8.4282(3) *c* = 5.9595(7)
180	Tetragonal *P*4/*mbm*	*a* = *b* = 8.4092(11) *c* = 5.9488(17)	Tetragonal *P*4/*mbm*	*a* = *b* = 8.42080(17) *c* = 5.9555(4)
160	Tetragonal *P*4/*mbm*	*a* = *b* = 8.4008(7) *c* = 5.9450(11)	Tetragonal *P*4/*mbm*	*a* = *b* = 8.40991(12) *c* = 5.9507(2)
140	Tetragonal *P*4/*mbm*	*a* = *b* = 8.3893(9) *c* = 5.9411(13)	Tetragonal *P*4/*mbm*	*a* = *b* = 8.40066(9) *c* = 5.95035(15)
120	Tetragonal *P*4/*mbm*	*a* = *b* = 8.3811(10) *c* = 5.9398(14)	Tetragonal *P*4/*mbm*	*a* = *b* = 8.38846(13) *c* = 5.9453(2)
80	Tetragonal *P*4/*mbm*	*a* = *b* = 8.3657(9) *c* = 5.9312(13)	Tetragonal *P*4/*mbm*	*a* = *b* = 8.37597(10) *c* = 5.93930(16)

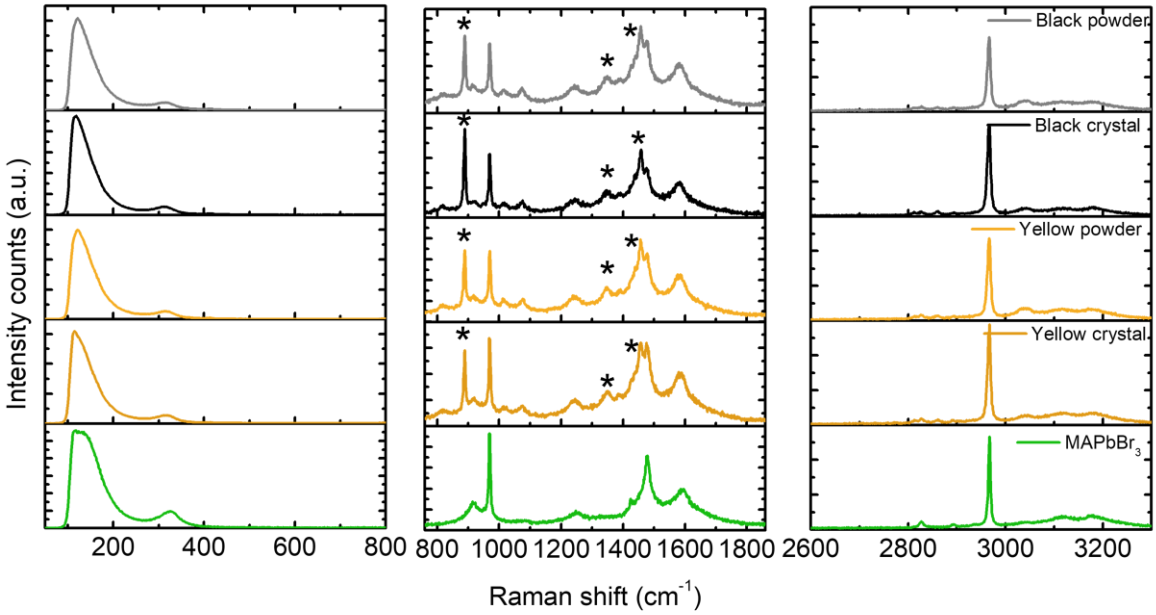

Figure S7. Representative Raman spectra collected in the 100-3200 cm^{-1} range showing the evolution of the MA and DMA vibrational modes, collected using 633 nm laser excitation at room temperature: $MAPbBr_3$ crystal, yellow crystal and powder, and black crystal and powder. The asterisks in the middle panel mark the Raman modes corresponding to DMA at 890 cm^{-1} (C-N-C stretching); 1350 cm^{-1} (CH_3 rocking); and 1461 cm^{-1} (CH_3 bending).[1–3]

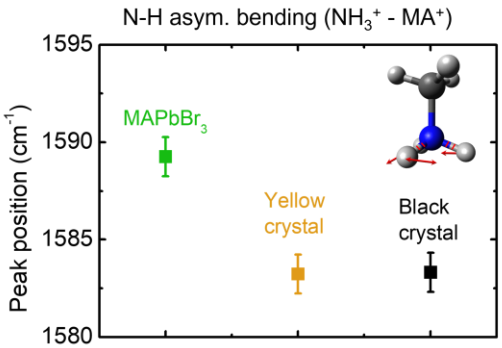

Figure S8. Peak positions corresponding to the N−H asymmetric bending mode in MA for the different crystals. Data averages from 5 different points for each sample is reported.

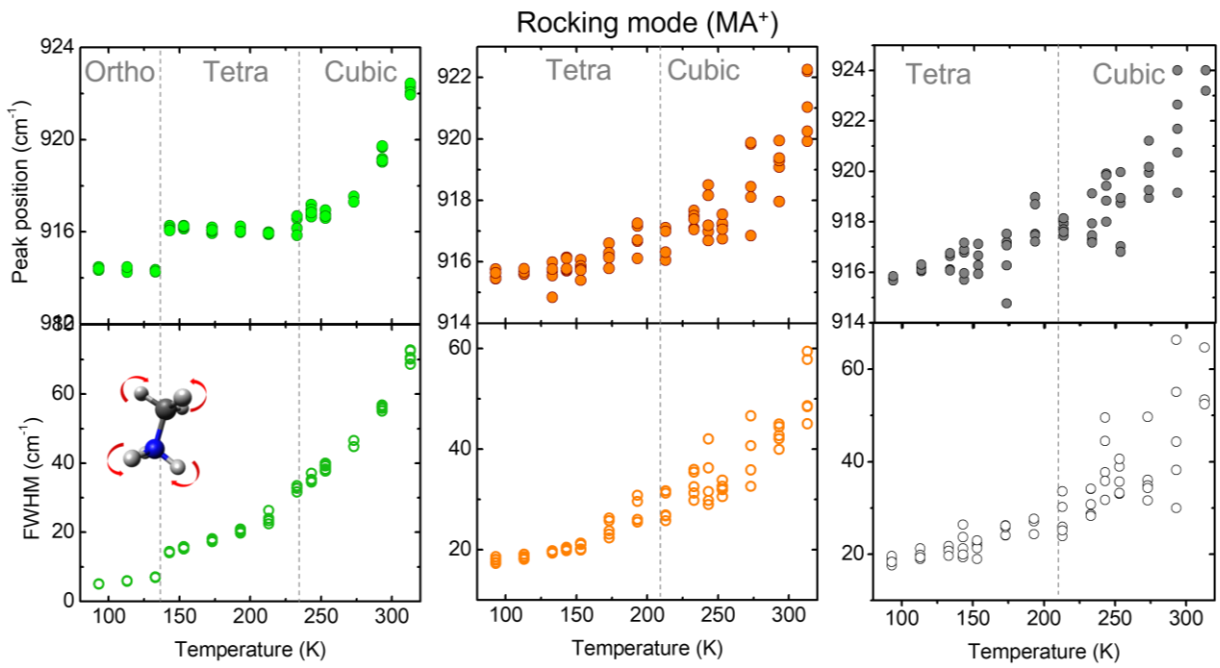

Figure S9. Temperature evolution of the Raman peak position (top panels) and full width at half maximum (bottom panels) of the rocking mode of MA[4–6] for pure $MAPbBr_3$ crystal (left), yellow crystal (middle), and black crystal (right). The dotted lines mark the phase transition temperatures. Sketches of the vibration modes drawn with Avogadro software[7] are shown as insets. The results shown are from 5 different points in each sample.

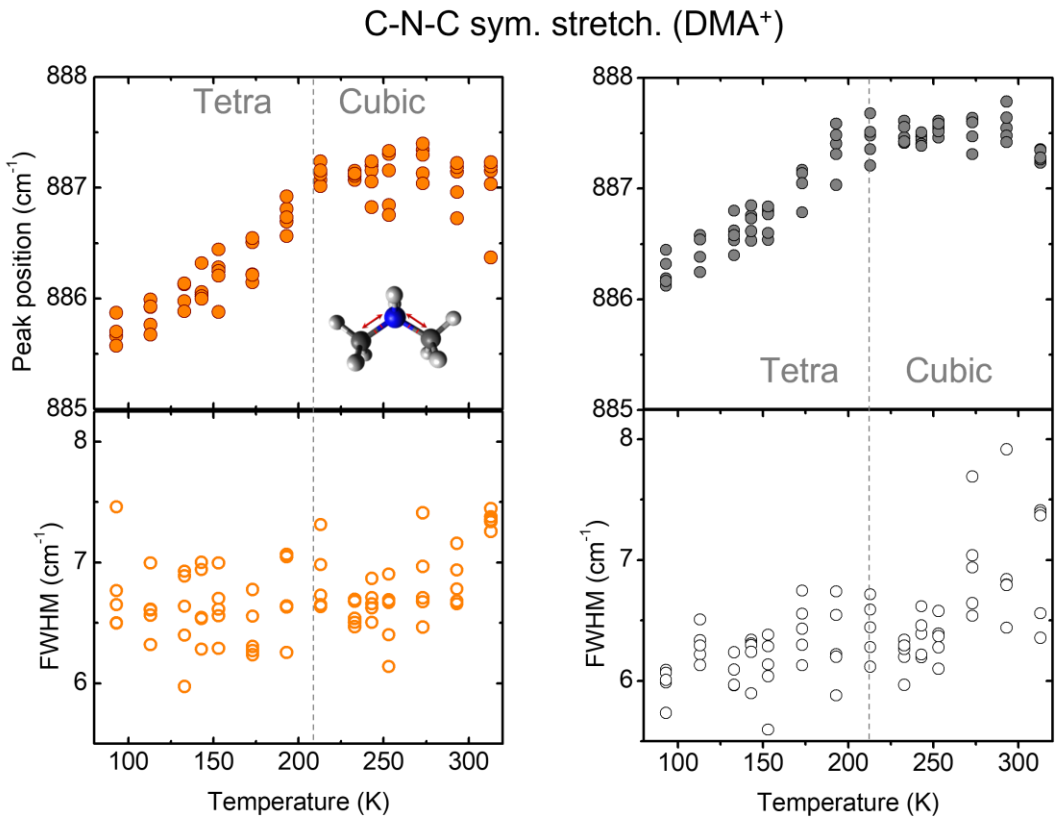

Figure S10. Temperature evolution of the Raman peak position (top panels) and full width at half maximum (bottom panels) of the symmetric stretching mode of DMA [1,2] for yellow crystal (left), and black crystal (right). The dotted lines mark the phase transition temperatures. Sketches of the vibration modes drawn with Avogadro software[7] are shown as insets. The results shown are from 5 different points for each sample.

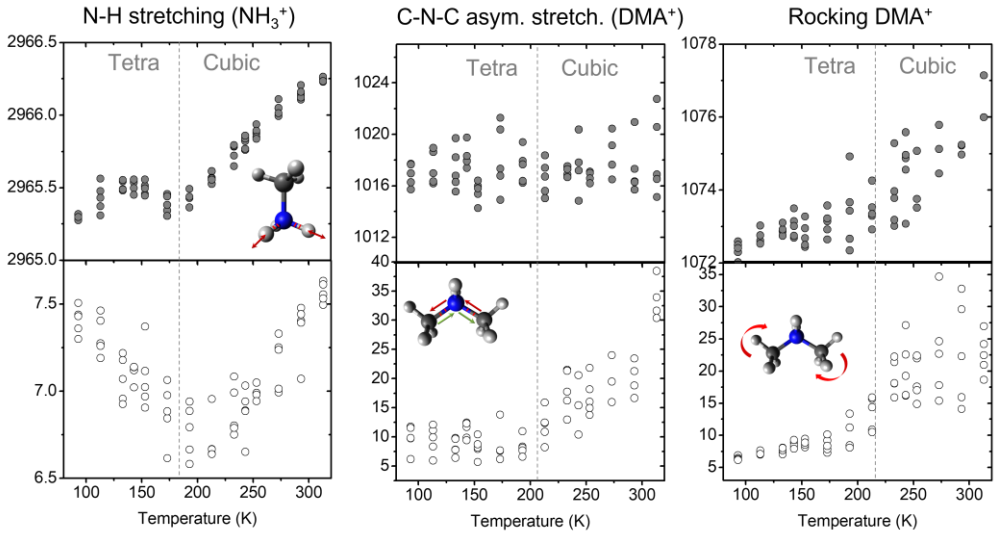

Figure S11. Temperature evolution of the Raman peak position (top panels) and full width at half maximum (bottom panels) for black crystal for the N-H stretching in MA[6], asymmetric stretching C-N-C in DMA and rocking of DMA^+ modes.[1–3] The dotted lines mark the phase transition temperatures. Sketches of the vibration modes drawn with Avogadro software are shown as insets. The results shown are from 8 different points in each sample.

Table S2. Position and FWHM of the rocking and stretching modes of MA at T = 93 K in the different crystals under study.

Raman mode	$MAPbBr_3$ crystals[3]	Yellow crystals[3]	Black crystals
MA Rocking mode	914 ± 0.1 cm^{-1} (FWHM 5 ± 1 cm^{-1})	916 ± 0.1 cm^{-1} (FWHM 18 ± 1 cm^{-1})	916 ± 0.1 cm^{-1} (FWHM 19 ± 1 cm^{-1})
C-N stretching	970 ± 0.1 cm^{-1} (FWHM 2.9 ± 0.1 cm^{-1})	972 ± 0.2 cm^{-1} (FWHM 7.5 ± 0.1 cm^{-1})	971 ± 0.1 cm^{-1} (FWHM 7.2 ± 0.1 cm^{-1})
C-H stretching mode (CH_3)	2820 ± 0.1 cm^{-1} (FWHM 3.1 ± 0.1 cm^{-1})	2823 ± 0.2 cm^{-1} (FWHM 7.7 ± 0.5 cm^{-1})	2824 ± 2 cm^{-1} (FWHM 8 ± 5 cm^{-1})
N-H stretching	2965 ± 0.1 cm^{-1} (FWHM 2.2 ± 0.1 cm^{-1})	2965 ± 0.1 cm^{-1} (FWHM 7.5 ± 0.1 cm^{-1})	2965 ± 0.1 cm^{-1} (FWHM 7.4 ± 0.1 cm^{-1})

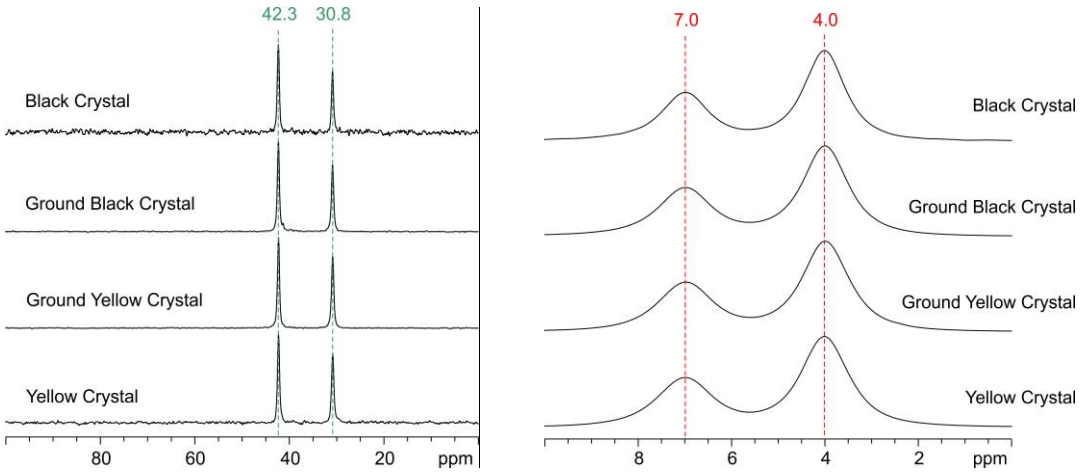

Figure S12. ^{13}C (100.64 MHz) CPMAS (left) and ^{1}H (400.23 MHz) MAS (right) SSNMR spectra of black and yellow crystals and their corresponding powders, acquired at 12 kHz at room temperature.

References

(1) Simenas, M.; Balciunas, S.; Wilson, J. N.; Svirskas, S.; Kinka, M.; Garbaras, A.; Kalendra, V.; Gagor, A.; Szewczyk, D.; Sieradzki, A.; Maczka, M.; Samulionis, V.; Walsh, A.; Grigalaitis, R.; Banys, J. Suppression of Phase Transitions and Glass Phase Signatures in Mixed Cation Halide Perovskites. *Nat. Commun.* **2020**, *11*, 1–9.

(2) Mączka, M.; Ptak, M. Simple, Fast and Non-Destructive Method for Detection of Dimethylammonium Impurity in Photovoltaic Methylammonium Lead Halides. *Appl. solid state Chem.* **2018**, *1*, 45–48.

(3) Ray, A.; Martín-García, B.; Moliterni, A.; Casati, N.; Boopathi, K. M.; Spirito, D.; Goldoni, L.; Prato, M.; Giacobbe, C.; Giannini, C.; Stasio, F. Di; Krahne, R.; Manna, L.; Abdelhady, A. L. Mixed Dimethylammonium/Methylammonium Lead Halide Perovskite Single Crystals for Improved Structural Stability and Enhanced Photodetection. *Adv. Mater.* **2021**, 34, 2106160.

(4) Wang, K.-H.; Li, L.-C.; Shellaiah, M.; Wen Sun, K. Structural and Photophysical Properties of Methylammonium Lead Tribromide ($MAPbBr_3$) Single Crystals. *Sci. Rep.* **2017**, *7*, 13643.

(5) Leguy, A. M. A.; Goñi, A. R.; Frost, J. M.; Skelton, J.; Brivio, F.; Rodríguez-Martínez, X.; Weber, O. J.; Pallipurath, A.; Alonso, M. I.; Campoy-Quiles, M.; Weller, M. T.; Nelson, J.; Walsh, A.; Barnes, P. R. F. Dynamic Disorder, Phonon Lifetimes, and the Assignment of Modes to the Vibrational Spectra of Methylammonium Lead Halide Perovskites. *Phys. Chem. Chem. Phys.* **2016**, *18*, 27051–27066.

(6) Yin, T.; Fang, Y.; Fan, X.; Zhang, B.; Kuo, J. L.; White, T. J.; Chow, G. M.; Yan, J.; Shen, Z. X.

Hydrogen-Bonding Evolution during the Polymorphic Transformations in $CH_3NH_3PbBr_3$: Experiment and Theory. *Chem. Mater.* **2017**, *29*, 5974–5981.

(7) Hanwell, M. D.; Curtis, D. E.; Lonie, D. C.; Vandermeerschd, T.; Zurek, E.; Hutchison, G. R. Avogadro: An Advanced Semantic Chemical Editor, Visualization, and Analysis Platform. *J. Cheminform.* **2012**, *4*, 17.